Tricolor Ho^{3+} Photoluminescence Enhancement from Site Symmetry Breakdown in Pyrochlore $Ho_2Sn_2O_7$ after Pressure Treatment

Yongsheng Zhao,[1] Kai Chen,[2] Nana Li,[1] Shuailing Ma,[1] Yonggang Wang,[1] Qingyu Kong,[3] Francois Baudelet,[3] Xin Wang,[4] and Wenge Yang[1,*]

[1]*Center for High Pressure Science and Technology Advanced Research (HPSTAR), Shanghai 201203, China*
[2]*Helmholtz-Zentrum Berlin für Materialien und Energie, Albert-Einstein-Strasse 15, 12489, Berlin, Germany*
[3]*Synchrotron SOLEIL, L'Orme des Merisiers, Saint-Aubin-BP48, 91192 Gif-sur-Yvette Cedex, France*
[4]*State Key Laboratory of Superhard Materials, Jilin University, Changchun 130012, China*

(Received 10 June 2020; accepted 2 November 2020; published 7 December 2020)

The photoluminescence (PL) characterization spectrum has been widely used to study the electronic energy levels. Ho^{3+} is one of the commonly used doping elements to provide the PL with concentration limited to 1% atomic ratio. Here, we present a tricolor PL achieved in pyrochlore $Ho_2Sn_2O_7$ through pressure treatment at room temperature, which makes a non-PL material to a strong multiband PL material with Ho^{3+} at the regular lattice site with 18.2% concentration. Under a high pressure compression-decompression treatment up to 78.0 GPa, the $Ho_2Sn_2O_7$ undergoes pyrochlore ($Fd3m$), to cotunnite ($Pnma$), then amorphous phase transition with different Ho^{3+} coordinations and site symmetries. The PL emerged from 31.2 GPa when the pyrochlore to cotunnite phase transition took place with the breakdown of site symmetry and enhanced hybridization of Ho^{3+} $4f$ and $5d$ orbitals. Upon decompression, the materials became an amorphous state with a partial retaining of the defected cotunnite phase, accompanied with a large enhancement of red-dominant tricolor PL from the ion pair cross-relaxation effect in the low-symmetry (C_1) site, in which two distinct Ho^{3+} emission centers (S center and L center) are present.

DOI: 10.1103/PhysRevLett.125.245701

Because of the high structural stability at extreme radiation, pressure, and temperature environment, the pyrochlore $A_2B_2O_7$ has been considered as an advanced nuclear material for nuclear reactors or waste immobilization in hostile environments [1–5]. It is crucial to extract the extreme condition history by checking the hostile materials. In recent years, much work has been devoted to identify the effect of pressure and temperature coupled with irradiation. A variation of novel behaviors such as phase transition, order-disorder transformation, recrystallization, and amorphization are observed, which provides important information [6–9]. However, few of these materials meet the criteria that the quenched materials can bring in the high pressure (HP) treatment history information which can be used as an extreme condition detector when combined with nuclear reaction materials as an inert matrix fuel.

Lanthanide compounds $Ln_2B_2O_7$ are excellent refractories while some Ln-containing ones exhibit interesting photoluminescence (PL) behavior which can act as a laser [10]. Most lanthanide ions can act as the PL center when doping in host materials due to their unique f-f and f-d transitions but with limited doping concentration (typically <1% atomic ratio) [11–13]. Most high concentrated lanthanide materials show no PL spectra due to the cross relaxation and energy transfer to nonradiative levels, which expedites the nonradiative deexcitation process and reduces the probability of radiative recombination [14]. We explored the PL evolution of concentrated materials $Eu_2Sn_2O_7$ and $La_2Sn_2O_7$ under pressure, and found that change of the local Eu^{3+} or Sn^{2+} site symmetry can largely explain the suppression and absence of PL [15,16]. The same situation was reported in Mn^{2+} doped BaF_2/SrF_2, MnF_2, and Cr_4PbBr_6 [17–19]. Inspired by this, the non-PL $Ho_2Sn_2O_7$ is selected and subjected to HP treatment to alter the local site symmetry. Surprisingly, Ho^{3+} PL is successfully generated by the pressure-induced phase transition, and upon decompression, the minority red emission is largely enhanced (fourfold) along with the other two bands due to the Ho^{3+} site symmetry breakdown and ion pair cross relaxation.

We carried out a systematic HP study on $Ho_2Sn_2O_7$, especially the PL measurements. In order to identify the Ho^{3+} site symmetry with pressure, *in situ* x-ray diffraction (XRD) and x-ray absorption spectroscopy (XAS) at Ho L_3 edge are performed. At an ambient condition, $Ho_2Sn_2O_7$ initially has no PL response due to high symmetry structure (centrosymmetry space group $Fd3m$). Pressure-induced tricolor visible PL was observed above 31.2 GPa [Fig. 1(a)], where the Ho^{3+} site symmetry changes from a centrosymmetry D_{3d} in LP $Fd3m$ *phase* to a non-centrosymmetry C_s in HP $Pnma$ phase (shown in Fig. 2). A similar structural phase transition induced PL was reported in MnF_2 and Cr_4PbBr_6 [18,19]. The tricolor PL in $Ho_2Sn_2O_7$ is largely enhanced under decompression,

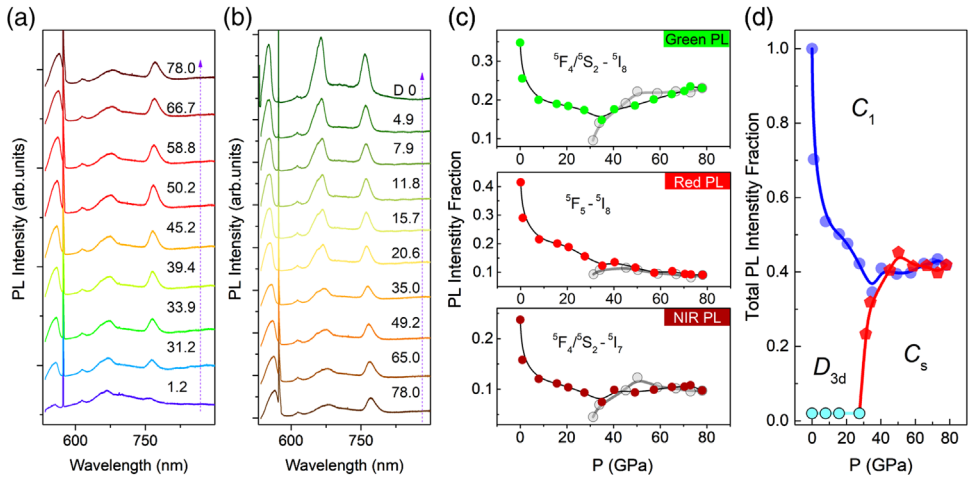

FIG. 1. (a) PL spectra of $Ho_2Sn_2O_7$ under compression. The sharp line is from the diamond Raman peak. (b) During decompression, the PL are enhanced, and the red PL becomes dominant. (c) The separated three PL intensity fractions normalized to the quenched total intensity with pressure. The gray circles represent compression data, while the color circles represent the decompression process. (d) Total PL intensity fraction during the compression and decompression process. The Ho^{3+} site symmetries are labeled (D_{3d}, C_s, and C_1) with the corresponding PL regions.

which is totally different with the quenched PL in the above samples due to their reversible phase transition. Once defects were formed in a pyrochlore compound, it would not easily relax back to the pristine structure [6,8]. That is why an intriguing tricolor PL is reserved in $Ho_2Sn_2O_7$ under decompression. More interestingly, the PL intensity is largely enhanced, especially the red PL, which is usually considered as a minority component is enhanced by four-fold [20]. The preservation and enhancement of the tricolor PL during decompression is attributed to the irreversible phase transition from the cotunnite phase which became an amorphous state with partial retaining of a defected cotunnite phase. Our results suggest that pressure is a crucial tool to transform a non-PL material $Ho_2Sn_2O_7$ into a PL system by altering the Ho^{3+} site symmetry.

There is no PL response at ambient pressure in $Ho_2Sn_2O_7$. A pressure-induced infrared-to-visible PL emerges above 31.2 GPa. It consists of three emission bands at 554 nm (green PL), 662 nm (red PL), and 763 nm [near infrared (NIR PL)] which are associated with Ho^{3+} ion radiative transition $^5F_4/^5S_2 \rightarrow {}^5I_8$, $^5F_5 \rightarrow {}^5I_8$, and $^5F_4/^5S_2 \rightarrow {}^5I_7$, respectively [21–23]. Upon further compression, the green and NIR PL intensities increase quickly with pressure below 50.2 GPa, and reach a plateau between 50.2 and 78.0 GPa, while the red PL remains almost constant as shown in Figs. 1(a) and 1(c). The pressure range

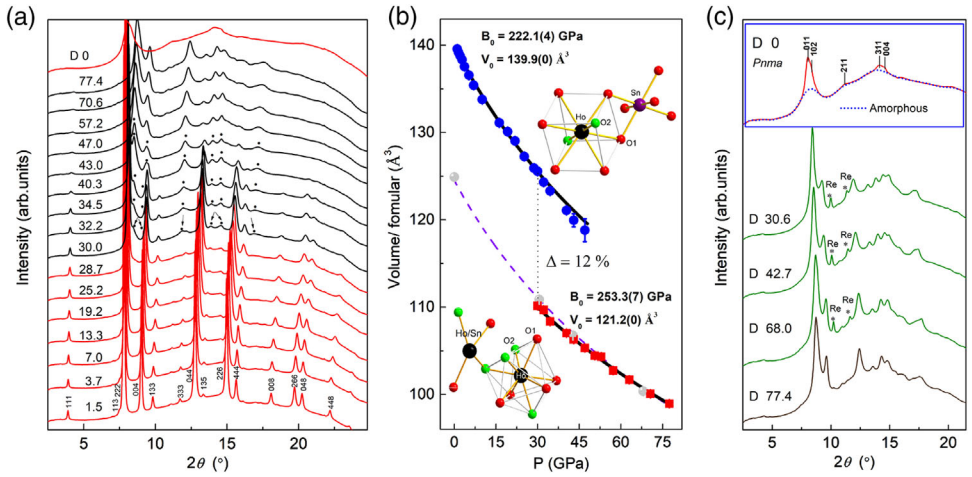

FIG. 2. Pressure-derived structure evolution in $Ho_2Sn_2O_7$. (a) The HP XRD patterns up to 77.4 GPa. (b) The P-V curve can be fitted with the Birch-Murnaghan equation of state which is separated by LP phase and HP phase. The inset shows the crystal structure of the LP phase (upper right) and HP phase (lower left). (c) The decompression XRD patterns. The star peaks are from the gasket.

31.2 GPa to 50.2 GPa is a transition zone from the cubic to orthorhombic (see XRD results in Fig. 2). More interesting is that the tricolor PL is not only retained but also largely enhanced upon decompression [Fig. 1(b)]. The pressure dependence of the PL intensity fractions of the three bands is plotted in Fig. 1(c) and the total PL fraction is shown in Fig. 1(d). Comparing with PL at 78.0 GPa, the quenched green PL and NIR PL intensities are almost doubled, while the red PL intensity increases fourfold and becomes dominant. This drastic change in light induced emission is governed by the pressure-induced site symmetry breakdown (see discussion in detail below).

In order to understand pressure-induced PL in $Ho_2Sn_2O_7$ and enhancement upon decompression, *in situ* HP XRD measurements are performed and selected patterns are presented in Fig. 2(a). Several new diffraction peaks appeared at 30.0 GPa, indicating the onset of the pressure-induced phase transition. At 50.2 GPa, the HP phase transition was completed. The symmetry changes from LP pyrochlore $Fd3m$ (O_h) to HP cotunnite $Pnma$ (D_{2h}) accompanied with a volume collapse about 12% as shown in Fig. 2(b) [8,24]. The detail Wyckoff position and Ho^{3+} site symmetry of LP phase and HP phase are listed in Table S1 in Supplemental Material [25]. Two P-V curves are fitted by the Birch-Murnaghan equation of state for LP and HP phases. A bulk modulus $B_0 = 222.1(4)$ GPa and volume $V_0 = 139.9(0)$ Å^3 are obtained below 30.0 GPa, while $B_0 = 253.3(7)$ GPa and $V_0 = 121.2(1)$ Å^3 above 47.0 GPa. Both LP and HP phases present between 30.0 and 47.0 GPa. The Ho^{3+} site symmetry changes from D_{3d} symmetry (HoO_8) in LP phase to C_s symmetry (HoO_9) in HP phase as shown in the insets of Fig. 2(b). Rietveld refinements of XRD patterns and the a, b, c vs pressure are shown in Figs. S1 and S2. Under decompression, the phase transition is irreversible as shown in Figs. 2(c) and S3 (Raman spectrum and Table S2), where the HP cotunnite phase reserved and coexisted with amorphous state (Ho^{3+} site with C_1 symmetry). For comparison, we also conducted the XRD and PL measurements by decompressing pressure from 29.0 GPa, and no-PL generated by the compression-decompression cycle (Fig. S4).

XAS of Ho L_3 edge ($E = 8.071$ keV) were measured to check the electronic state change associated with the structure phase transition to 40.5 GPa. The original XAS, derivative, and second derivative near the white line energy 8.071 keV are plotted in Fig. S5. Two purple lines in Fig. S5b connect the local maximum and minimum near the white line in the derivative of XAS at varied pressures. As pressure increases, the white line gets broader (Fig. S5a). The constant edge jumping positions (first purple line) at different pressures suggest for an unchanged Ho^{3+} with $4f^{10}$ electron configuration in $Ho_2Sn_2O_7$. The shift to higher energy with pressure on the local minimum (second purple line position) results from the reduced first shell Ho-O bonding length. The detail second derivatives of the Ho

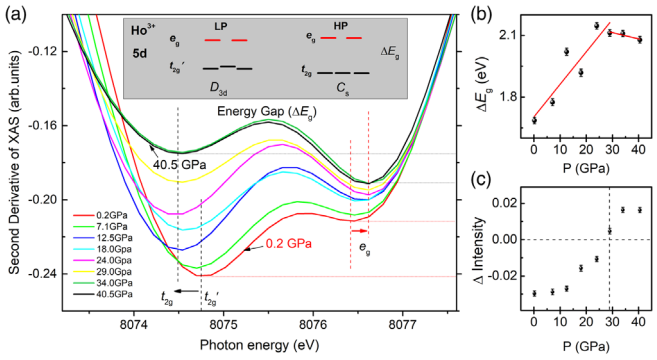

FIG. 3. (a) The second derivative of XAS measured under various pressures. The inset shows the energy gap ΔE_g with pressure. (b) Energy gap ΔE_g variation with pressure. (c) The relative intensity of $[e_g - t'_{2g}(t_{2g})]$ with pressure.

L_3-edge XAS spectra are shown in Fig. 3(a), the W-shape feature illustrates the energy level of Ho^{3+} $5d$ orbitals. The two minimum positions correspond to the energy levels of t_{2g} and e_g as depicted in the inset in Fig. 3(a). Similar to the spectra of W and Mo [26,27], the energy separation represents the splitting of the Ho_{5d}-O_{2p} orbitals into t_{2g} and e_g by the ligand field of the surrounding oxygen atoms, and the e_g orbitals have higher energies than those of t_{2g} orbitals when a simply O_h symmetry is considered (Fig. 4). The t_{2g} orbitals of Ho^{3+} ions with D_{3d} site symmetry distortion at low pressure splits into a_{1g} and e_{2g} (t'_{2g}), while at HP with C_s site symmetry, the t_{2g} degenerates to one energy level with the crystal field splitting energy $\Delta = 10$ Dq. As shown in Fig. 3(b), the energy gap ΔE_g between the t'_{2g} (or t_{2g}) and e_g of the hybridized Ho_{5d}-O_{2p} states, behaves differently at pressure below and above 29.0 GPa, where the phase transition takes place. ΔE_g increases from ~1.7 eV at 0.2 GPa to ~2.1 eV at 24.0 GPa, and keeps almost unchanged up to 40.5 GPa. Besides, the relative intensities of the t'_{2g} (or t_{2g}) and e_g peaks connect to the number of unoccupation at t'_{2g} (or t_{2g}) and e_g orbit [Fig. 3(c)]. The decreasing intensity at the t_{2g} peak indicates a crossover of electron occupation from e_g to t_{2g} through the phase transition. Because of increasing the crystal field splitting energy to 10 Dq between the t_{2g} and e_g orbital, it is reasonable that the t_{2g} orbital of the Ho_{5d}-O_{2p} state would be more occupied in the HP cotunnite phase. The Ho^{3+} local site symmetry change from D_{3d} to C_s would bring in the emerging of tricolor PL [28].

The absence of PL in ambient $Ho_2Sn_2O_7$ is due to the Ho^{3+} site centrosymmetry (D_{3d}), in which the electric-dipole transition is forbidden. In the HP cotunnite phase, the Ho^{3+} site becomes noncentrosymmetric (C_s), which allows the electric-dipole radiative transition, enhances the quantum yields for all three bands in the LP-HP transition zone, and reaches a plateau once the transition is completed [12,29,30]. Upon decompression, the tricolor PL is reserved and largely enhanced, especially the red PL. The green PL and NIR PL almost double the intensity compared with that at 78.0 GPa,

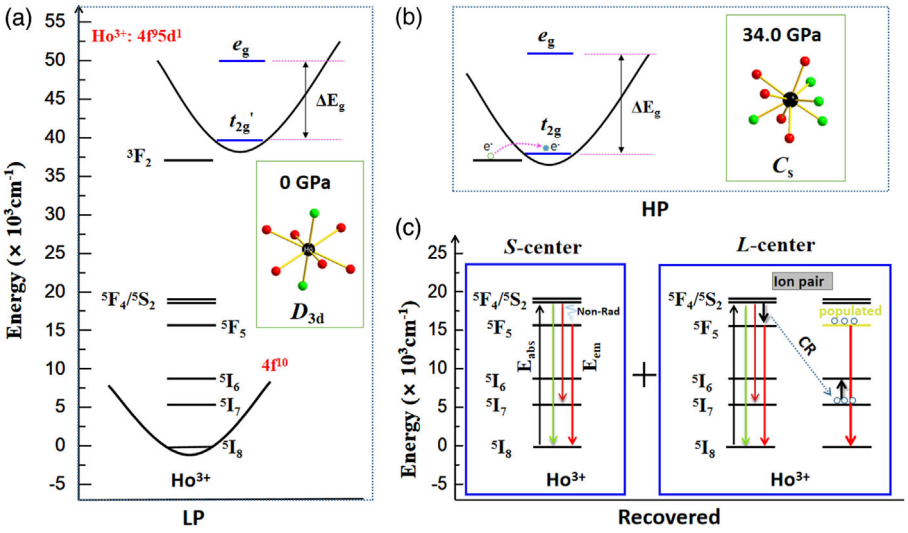

FIG. 4. The $5d$ orbital energy gap ΔE_g of Ho^{3+} ions between e_g and $t'_{2g}(t_{2g})$ at LP phase (a) and HP phase (b). The insets show the 0 GPa and 34.0 GPa site symmetry of Ho^{3+}, respectively. (c) Energy level diagram of Ho^{3+} under decompression, two emission centers of S center and L center are presented respectively. The energy transfer from Ho^{3+} ion-pair cross relaxation (CR) at the L center expedites the $^5F_5$ population and hence enhances the $^5F_5$ to $^5I_8$ radiation.

while the red PL enhances fourfold and becomes dominant. The reserved and enhanced PL is due to the low-site symmetry (C_1) in the amorphous and defect-HP phase which extremely promotes the radiative transition rate. As depicted in Fig. 4(b), the lowered t_{2g} orbital energy level allows the $4f$ electrons hopping into $5d$ orbital due to the enhanced hybridization of Ho^{3+} $4f$ and $5d$ orbitals in the site noncentrosymmetry C_s, where the S-center emission takes place as shown in Fig. 4(c). The dominant emission $^5F_4/^5S_2 \rightarrow {}^5I_8$ (green PL) is accompanied with weak NIR PL ($^5F_4/^5S_2 \rightarrow {}^5I_7$) and red PL ($^5F_5 \rightarrow {}^5I_8$). The electron occupation at $^5F_5$ depends on the nonradiation process, therefore the $^5F_5$ to $^5I_8$ radiation process has been considered as a minority component [20]. Upon decompression, the cotunnite phase is not stable and most $Ho_2Sn_2O_7$ transforms to an amorphous state with the retention of a small amount of the defect-cotunnite phase. In the totally released amorphous state, the strongly coupled Ho^{3+} pairs can exchange energy via the cross-relaxation process as shown in Fig. 4(c) L center: one Ho^{3+} ($^5S_2/^5F_4 \rightarrow {}^5F_5$), and the other Ho^{3+} ($^5I_7 \rightarrow {}^5I_6$), which expedites the $^5S_2/^5F_4 \rightarrow {}^5F_5$ radiation compared to the nonradiation mode in the S center model, and leads to the buildup of Ho^{3+} ($^5F_5$) population as shown in Fig. 4(c)[31,32]. The electrons at $^5I_7$ originated the from the $^5F_4/^5S_2 \rightarrow {}^5I_7$ transition. Therefore, the stronger recovered red PL ($^5F_5 \rightarrow {}^5I_8$) originates from two emission centers of Ho^{3+}, and the S center contributes the same intensity with green and NIR PL, while the L center contributes to the population of the $^5F_5$ energy level and enhanced $^5F_5 \rightarrow {}^5I_8$ (red) radiation rate. The strong two-color PL is very rare except as observed in some quantum dot materials and MnF_2 [33,34]. Here, the pressure treated $Ho_2Sn_2O_7$ presents a unique application in highly efficient yields of tricolor PL covering the range from green to red to NIR. Besides, the red and NIR spectral ranges are considered as the potential "optical windows" candidate for biological tissues [35].

In summary, under pressure the LP pyrochlore phase transformed to the HP cotunnite phase at 32.3 GPa in $Ho_2Sn_2O_7$. The increasing crystal field splitting between the t_{2g} and e_g causes the strong hybridization of $4f$ and $5d$ orbitals at the HP phase. Upon releasing pressure, the HP phase transforms to the coexistence of an amorphous and defect-cotunnite phase. The local Ho^{3+} site symmetry breaks down sequentially from D_{3d} to C_s then C_1, and nearest coordinations change accordingly. The pristine non-PL character in $Ho_2Sn_2O_7$ is popular as typically Ln^{3+} doped materials show PL spectrum with doping limitation up of 1%. Tricolor PL (S center) is successfully generated once the LP-HP phase transition starts and the site symmetry breaks down from D_{3d} to C_s. Decompression-induced amorphization reduces Ho^{3+} site symmetry further down to C_1, which enhances the ion pair cross-relaxation process and provides an additional emission center (L center) for the $^5F_5 \rightarrow {}^5I_8$ transition and promotes the minority red-PL to dominant among the tricolor PL. With compression up to 29.0 GPa, the quenched sample shows no PL change, which can be used as a pressure history detector for an extreme environment. Our findings highlight the role of the pressure effect on $Ho_2Sn_2O_7$; the reserved and enhanced tricolor PL can serve as the extreme condition history detector and improve bioluminescence imaging technology.

This work was financially supported by the National Nature Science Foundation of China (Grants No. U1930401, No. 51527801, and No. 51772184) and

National Key R&D Program of China (Grant No. 2017YFA0403401). HPCAT operations are supported by DOE-NNSA under Award No. DE-NA0001974, with partial instrumentation funding by NSF. The Advanced Photon Source (APS) is supported by DOE BES, under Contract No. DE-AC02-06CH11357 by UChicago Argonne, LLC.

*Corresponding author.
yangwg@hpstar.ac.cn

[1] R. W. Grimes, R. J. M. Konings, and L. Edwards, Nat. Mater. **7**, 683 (2008).
[2] J. S. Gardner, M. J. P. Gingras, and J. E. Greedan, Rev. Mod. Phys. **82**, 53 (2010).
[3] K. Sickafus, L. Minervini, R. Grimes, J. Valdez, M. Ishimaru, F. Li, K. McClellan, and T. Hartmann, Science **289**, 748 (2000).
[4] K. E. Sickafus, R. W. Grimes, J. A. Valdez, A. Cleave, M. Tang, M. Ishimaru, S. M. Corish, C. R. Stanek, and B. P. Uberuaga, Nat. Mater. **6**, 217 (2007).
[5] M. Subramanian, G. Aravamudan, and G. Subba Rao, Prog. Solid State Chem. **15**, 55 (1983).
[6] F. Zhang, J. Wang, J. Lian, M. Lang, U. Becker, and R. Ewing, Phys. Rev. Lett. **100**, 045503 (2008).
[7] S. Saha, S. Singh, B. Dkhil, S. Dhar, R. Suryanarayanan, G. Dhalenne, A. Revcolevschi, and A. Sood, Phys. Rev. B **78**, 214102 (2008).
[8] F. Zhang, M. Lang, Z. Liu, and R. Ewing, Phys. Rev. Lett. **105**, 015503 (2010).
[9] I. Mirebeau, I. Goncharenko, P. Cadavez-Peres, S. Bramwell, M. Gingras, and J. Gardner, Nature (London) **420**, 54 (2002).
[10] B. Wu, M. Zinkevich, C. Wang, and F. Aldinger, Rare Met. Cement. Carbides **25**, 549 (2006).
[11] C. Gong *et al.*, J. Phys. Chem. C **118**, 22739 (2014).
[12] W. M. Yen and H. Yamamoto, *Phosphor Handbook* (CRC press, Boca Raton, FL, 2006).
[13] Z. T. Chen, E. H. Song, M. Wu, S. Ding, S. Ye, and Q. Y. Zhang, J. Alloys Compd. **667**, 134 (2016).
[14] W. Yi, L. Langsheng, Z. Huiqun, and D. Ruiqin, Journal of rare earths / Chinese Society of Rare Earths **24**, 199 (2006).
[15] Y. Zhao, W. Yang, N. Li, Y. Li, R. Tang, H. Li, H. Zhu, P. Zhu, and X. Wang, J. Phys. Chem. C **120**, 9436 (2016).
[16] Y. Zhao, N. Li, C. Xu, Y. Li, H. Zhu, P. Zhu, X. Wang, and W. Yang, Adv. Mater. **29**, 1701513 (2017).
[17] I. Hernández and F. Rodríguez, Phys. Rev. B **67**, 012101 (2003).
[18] I. Hernández, F. Rodríguez, and H. D. Hochheimer, Phys. Rev. Lett. **99**, 027403 (2007).
[19] Z. Ma *et al.*, Nat. Commun. **9**, 4506 (2018).
[20] M. Mujaji, G. D. Jones, and R. W. G. Syme, Phys. Rev. B **48**, 710 (1993).
[21] A. Pandey and H. C. Swart, J. Lumin. **169**, 93 (2016).
[22] J. Yu, Y. Yang, R. Fan, D. Liu, L. Wei, S. Chen, L. Li, B. Yang, and W. Cao, Inorg. Chem. **53**, 8045 (2014).
[23] A. Pandey, V. Kumar, S. Som, A. Yousif, R. E. Kroon, E. Coetsee, and H. C. Swart, Appl. Surf. Sci. **423**, 1169 (2017).
[24] H. Y. Xiao, F. Gao, and W. J. Weber, Phys. Rev. B **80**, 212102 (2009).
[25] See Supplemental Material at http://link.aps.org/supplemental/10.1103/PhysRevLett.125.245701 for the experimental details and the additional results of XRD, Raman, and XAS of Ho L_3 absorption edge at high pressure.
[26] U. Jayarathne, P. Chandrasekaran, A. F. Greene, J. T. Mague, S. DeBeer, K. M. Lancaster, S. Sproules, and J. P. Donahue, Inorg. Chem. **53**, 8230 (2014).
[27] S. R. Bare, G. E. Mitchell, J. J. Maj, G. E. Vrieland, and J. L. Gland, J. Phys. Chem. **97**, 6048 (1993).
[28] J. A. Barreda-Argüeso, F. Aguado, J. González, R. Valiente, L. Nataf, M. N. Sanz-Ortiz, and F. Rodríguez, *J. Phys. Conf. Ser.* 950, 042016 (2017).
[29] D. Tu, Y. Liu, H. Zhu, R. Li, L. Liu, and X. Chen, Angew. Chem. Int. Ed. **52**, 1128 (2013).
[30] Y. Zhang, J. Hao, C. L. Mak, and X. Wei, Opt. Express **19**, 1824 (2011).
[31] N. M. Sangeetha and F. C. J. M. van Veggel, J. Phys. Chem. C **113**, 14702 (2009).
[32] A. S. Gouveia-Neto, E. B. da Costa, L. A. Bueno, and S. J. L. Ribeiro, J. Lumin. **110**, 79 (2004).
[33] C. Galland, S. Brovelli, W. K. Bae, L. A. Padilha, F. Meinardi, and V. I. Klimov, Nano Lett. **13**, 321 (2013).
[34] A. M. Dennis *et al.*, Adv. Funct. Mater. **29**, 1809111 (2019).
[35] J. Chu *et al.*, Nat. Biotechnol. **34**, 760 (2016).